

Magneto-Electric Interactions in Composites of Ferrite Films on Lattice-Matched Substrates and Ferroelectrics

Peng Zhou,^{1,2} Amit V. Singh,³ Z. Li,³ M. A. Popov,^{1,4} Ying Liu,^{1,2} D. A. Filippov,⁵ Tianjin Zhang,² Wei Zhang,¹ P. J. Shah,⁶ B. M. Howe,⁶ M. E. McConney,⁶ G. Srinivasan,^{1,6 a)} M. R. Page,^{6,b)} and A. Gupta^{3,c)}

¹ *Physics Department, Oakland University, Rochester, MI 48309, USA*

² *Department of Materials Science and Engineering, Hubei University, Wuhan 430062, China*

³ *Center for Materials for Information Technology, The University of Alabama, Tuscaloosa, AL 3548, USA*

⁴ *Faculty of Radiophysics, Electronics and Computer Systems, Taras Shevchenko National University of Kyiv, Kyiv, 01601, Ukraine*

⁵ *Novgorod State University, Veliky Novgorod, 173003 Russia*

⁶ *Materials and Manufacturing Directorate, Air Force Research Laboratory, Wright-Patterson Air Force Base, Dayton, OH 45433, USA*

Abstract

The nature of mechanical strain-mediated converse magnetoelectric effect (CME) has been studied in multiferroic composites of single-crystal like thin films of nickel ferrite (NFO) and polycrystalline lead zirconate titanate (PZT). Ferrite films of thickness 0.45 to 1 micron were prepared by Pulsed Laser Deposition on lattice-matched (100) and (110) substrates of magnesium gallate (MGO) and cobalt gallate (CGO) that resulted in elimination of antiphase boundaries and magnetic parameters comparable to bulk single crystals. Ferromagnetic resonance under a static electric field E was utilized for studies of CME effects in composites of PZT and NFO films on the substrates. The in-plane static magnetic field H was applied along the principal crystallographic axes of the ferrite film to study its influence on CME. The E -induced ME anisotropy field H_{ME} was estimated from FMR data based on shift in

resonance frequency with E in order to determine the ME constant $A = H_{ME}/E$. In composites with NFO films on (110) substrates (i) the ME coupling was stronger for films on CGO possibly due to a better lattice match and weaker substrate clamping than for films on MGO, (ii) A -values were the highest for $H // [1,-1,0]$, and (iii) a negative A -value was inferred for $H // [001]$. For composites with NFO on (100) substrates the strongest ME coupling was measured for H along $[001]$. A first model for CME that takes into consideration both compressive and bending deformation in the composites is developed and results of the theory are in agreement with both the sign and magnitude of the measured ME coefficient A . The results of the studies presented here indicate the potential for use of the composites in self-biased E -tunable microwave devices.

Authors to whom correspondence should be addressed:

^a srinivas@oakland.edu; ^b michael.page.16@us.af.mil; ^c agupta@mint.ua.edu,

1. Introduction

The nature of mechanical strain mediated electromagnetic coupling in composites of ferromagnetic-ferroelectric/piezoelectric phases is of fundamental and technological importance [1-5]. A variety of composites were studied in recent years. These include the use of ferromagnetic metals, alloys or ferrites for the magnetic phase and barium titanate, lead zirconate titanate (PZT), lead magnesium niobate-lead titanate (PMN-PT), AlN, and quartz for the ferroelectric/piezoelectric phase [6-10]. The strength of magneto-electric (ME) coupling between the two phases is studied by their response to an applied magnetic field H or an electric field E . Several of these systems were reported to show a strong ME coupling when subjected to H - or E -field at low-frequencies and at frequencies corresponding to resonance modes. The composites are of interest for a variety of sensors and high frequency devices [11-15]. Device efforts so far include magnetic sensors [16-18], gyrators capable of direct conversion of current-to-voltage [11, 19], tunable inductors [20], memory devices [10], and dual electric and magnetic field tunable high frequency devices [21-24].

Ferrite-ferroelectric composites, in particular, are of importance for signal processing devices at microwave and millimeter wave frequencies [23]. Interests in these systems evolved from studies of the converse ME (CME) effects, i.e., magnetic response of the composite to a static E -field [2,4,7]. The strength of CME is measured either from data on magnetization M versus H under E or tuning of ferromagnetic resonance (FMR) with E [25]. The piezoelectric strain in the ferroelectric phase is transferred to the ferrite and manifests as an induced magnetization or an anisotropy field H_{ME} . Thus CME will result in a shift in the

FMR resonance field (or frequency f_r) and data on H_{ME} or f_r vs E could be used to estimate the strength A of CME given by $A = H_{ME}/E$.

The converse ME effect under FMR in ferrite-ferroelectric composites, therefore, is attractive for realizing E -tunable microwave ferrite devices such as resonators and filters [23]. Ferrite devices, in general, are tuned with a magnetic field that requires high power for operation and H -tuning is generally slow and noisy and the devices cannot be miniaturized or integrated with semiconductor devices. Voltage tuning of the device is possible when a ferrite-ferroelectric composite is used. The converse-ME coefficient $A \sim \lambda d/M_s$ where λ and M_s are the magnetostriction and saturation magnetization, respectively, and d is the piezoelectric coupling coefficient. Thus, the key ingredients for strong CME and broad-band E -tunable devices are composites with high λ and d and small M_s . An equally important parameter is the FMR linewidth ΔH that must be much smaller than H_{ME} for practical devices.

This report is on CME effects in composites with single crystal-like epitaxial thin films of nickel ferrite, NiFe_2O_4 (NFO), with a large λ and a much smaller ΔH than bulk single crystals [26-28]. Recent significant efforts in this regard by subsets of the present authors include (i) observation of ΔH as low as 5 Oe, strain-induced uniaxial anisotropy field H_u of 10 kOe due to strong magnetoelastic interactions, and $\lambda \sim 10$ ppm for Pulsed Laser Deposited (PLD) NiZnAl - (NZAFO) ferrite films on MgAl_2O_4 (MAO) substrates [26,27], and (ii) PLD films of NFO on MAO, MgGa_2O_4 (MGO) and CoGa_2O_4 (CGO) substrates with $H_u \sim 0.5$ -11.9 kOe and $\Delta H \sim 25$ Oe [28]. The smallest ΔH and highest H_u were measured for NFO films on MGO and CGO substrates with a film-lattice mismatch of 0.8% and 0.2%, respectively, and was attributed to the elimination of undesired anti-phase boundary defects and the influence of

strain in the films. This unique combination of low- ΔH and high- H_u make both the NZAFO- and NFO- films highly desirable for possible use in E -tunable ferrite-ferroelectric microwave and millimeter wave devices [26,28].

Here we discuss results of our studies on CME effects in composites of PZT and NFO films on (100) and (110) substrates of MGO and CGO. Films of thickness 450 nm – 1 μ m were grown by PLD and characterized by structural and magnetic measurements. Magnetization and FMR measurements on the films on (100) and (110)-oriented MGO substrates with lattice mismatch of 0.8% showed a large easy plane anisotropy field. The films on CGO substrates with a smaller lattice mismatch of 0.2% also showed an easy plane anisotropy field, but was much smaller than for films on MGO. The strength of the CME coupling in epoxy bonded composites of PZT and the NFO films on MGO and CGO substrates was estimated from data on shift in the FMR frequency due to a static E -field applied to PZT. Measurements were done for in-plane H parallel to [001] or [011] for NFO films on (100) substrates and for H along the 3 principal axes for (110) films. The anisotropy field H_{ME} due to ME interactions was estimated from the FMR data and the ME coefficient $A = H_{ME}/E$ was determined. For composites with (110) NFO films the CME coupling coefficient A was the highest for H along [0,-1,1] axis, whereas for (100) NFO films the CME coupling was strongest for H along [001]. A model has been developed for the CME effects. It was essential to consider both the compressive and bending deformations under the applied fields in to account for the sign and magnitude of A . Estimated A -values are in good agreement with the data. The NFO-PZT composites discussed here show one of the strongest ME coupling reported so far and are of interest for use in dual E - and H -tunable microwave ferrite devices. The observation of a

very high growth induced anisotropy field in the ferrite films, in particular, is significant for use of the ferrite films in composites for miniature, self-biased resonators and filters and for possible integration with semiconductor devices.

2. Experiment

Nickel ferrite, NiFe_2O_4 (NFO), films were deposited on (100) or (110)-oriented MGO and CGO substrates ($5 \times 5 \times 0.5 \text{ mm}^3$) by PLD technique in an oxygen environment with a background pressure of 10 mTorr. The laser fluence was set to $\sim 1 \text{ J/cm}^2$ and the temperature of the substrates was maintained at 700°C during film growth. Figure 1 shows the normal θ - 2θ x-ray scans around the (400) and (440) peaks of the NFO and the substrate for films grown on MGO and CGO with (100) and (110) orientations, respectively. A relatively large gap between the film and substrate peak positions is observed for NFO//MGO samples of both orientations, while the film peaks are essentially merged with the left shoulder of the substrate peaks for both the NFO//CGO samples. This indicates that the NFO//CGO films have lower lattice mismatch than the NFO//MGO films.

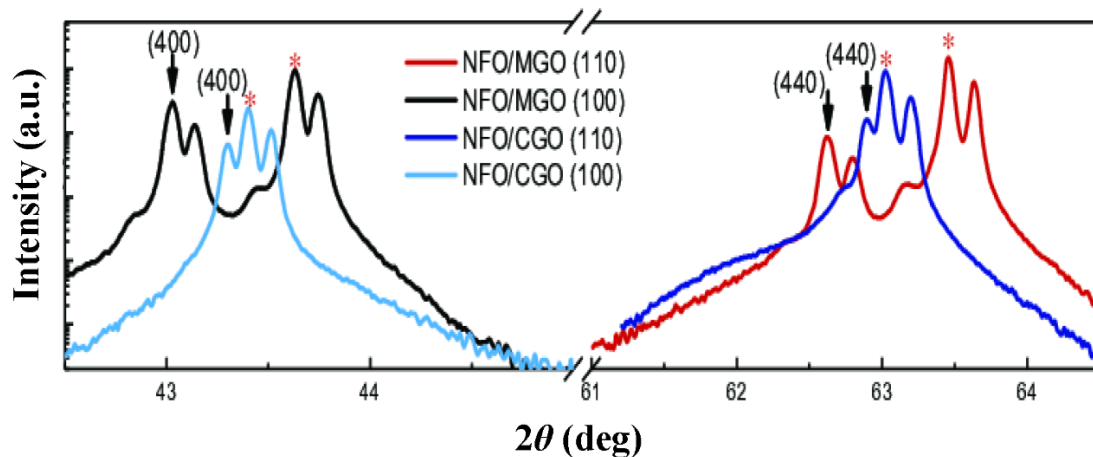


Fig. 1: Normal θ - 2θ x-ray diffraction patterns for NiFe_2O_4 films grown on (100) and (110)-oriented MgGa_2O_4 (MGO) and CoGa_2O_4 (CGO) substrates (peak positions marked with *). The plots show only the scan range around the (400) and (440) peaks for the respective films and substrates. The splitting of the peaks for the films and substrates arise from $\text{Cu-K}_{\alpha 1}$ and $\text{Cu-K}_{\alpha 2}$ X-ray radiation wavelengths.

Magnetization measurements were performed on NFO films grown on (100) or (110)-oriented MGO and CGO to examine their hysteresis characteristics and magnetic anisotropy. As shown in Fig. 2(a, b) for NFO//MGO (100) and NFO//CGO (100) thin films, the hysteresis loops for the normalized magnetization measured along the [010] and [001] directions are essentially identical, with sharp switching followed by more gradual increase (decrease) to saturation at fields $\sim \pm 0.5$ kOe. The hysteresis loop in the diagonal [011] direction exhibits a sharper saturation of the magnetization, corresponding to the in-plane easy axis direction. The (100)- films on both substrates exhibit fourfold anisotropy. In contrast, for the NFO//MGO (110) film (Fig. 2c) a sharp switching of the magnetization is observed when H is applied along the [1-10] direction. However, with H applied along the [001] direction, a magnetic hard axis switching behavior is obtained with an anisotropy field of ~ 1500 Oe. As a comparison, Fig.2(d)

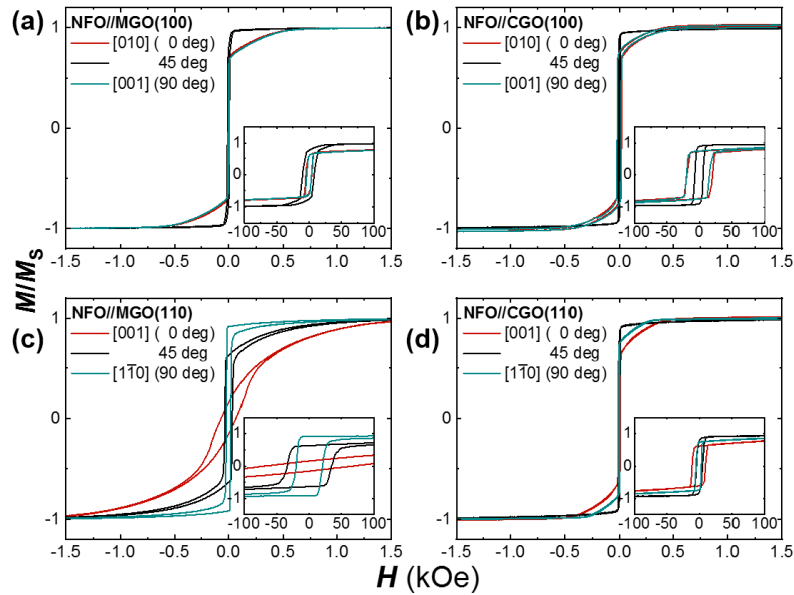


Fig. 2: (a) and (b) Normalized in-plane magnetization versus H plots for NFO//MGO (100) and NFO//CGO (100), respectively. The magnetization for 450 nm thick ferrite films is measured with the in-plane H oriented in two orthogonal directions ([001], [010]) and in the diagonal direction ([011]). (c) and (d) Normalized in-plane magnetization versus H for NFO//MGO (110) and NFO//CGO (110), respectively. The magnetization is measured with an external in-plane H applied in two perpendicular directions ([001], [1-10]) and in the diagonal direction ([1-11]).

shows the magnetization result for NFO//CGO (110) thin film. For this sample, the shapes of magnetization loops in the two perpendicular directions are similar or even overlap with each other, which is quite different from the NFO//MGO (110) sample. The results for the NFO//MGO (110) thin film indicates the presence of a strong in-plane uniaxial anisotropy in addition to the fourfold magnetocrystalline anisotropy observed for NFO//MGO (100). On the other hand, for NFO//CGO (011) thin film, the fourfold anisotropy is dominant and only a weak uniaxial anisotropy is present. Thus, we conclude that significant magnetic strain anisotropy exists in NFO//MGO (110) thin film due to a large lattice mismatch between film and substrate, while no significant strain anisotropy is noted in the NFO//CGO (110) film because of the much smaller mismatch.

Ferromagnetic resonance measurements were done with the sample placed in a coplanar waveguide and subjected to an in-plane field H . Resonance profiles were recorded both by (i) using a vectoring network analyzer to measure the scattering matrix parameter S_{21} versus frequency f for a constant H (Fig.3a), and (ii) using magnetic field modulation to record the derivative of the power absorbed dP/dH as a function of H at a fixed f as shown in Fig.3(b).

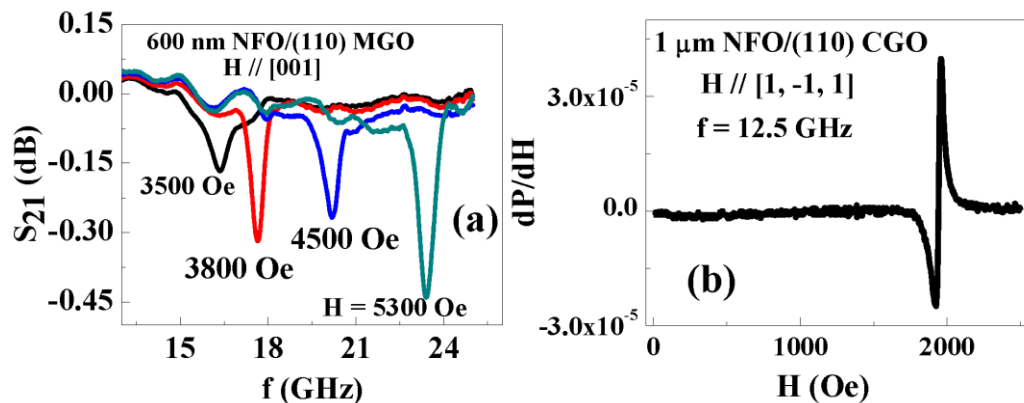


Fig.3. Representative ferromagnetic resonance (FMR) profiles for nickel ferrite (NFO) films. (a) Scattering matrix S_{21} vs frequency f showing FMR for a series of bias field H for NFO on (110) MGO substrate. (b) Derivative of power absorbed dP/dH versus H showing FMR for a 1 μm thick NFO film on (110) CGO substrate.

The FMR measurements were done as a function of the orientation of H relative to the [001] axis for both (100) and (110) films of NFO on MGO and CGO. Data on resonance field or frequency were used to estimate the magnetic parameters for the films as discussed in the subsequent sections. The FMR line-width ΔH varied from a minimum of 25 Oe to a maximum of 50 Oe, depending on the frequency, substrate material and orientation and were consistent with reported values for NFO films on (100) MGO and CGO [28].

3. Converse Magneto-Electric Effects

3.1. Composites of PZT and NFO film on (110) MGO substrates

Pre-poled, vendor supplied polycrystalline PZT (#APC-850, American Piezo-Ceramics, PA) of thickness 0.2 - 0.3 mm with silver electrodes were used. NFO films on the substrates were cut to dimensions $4 \times 4 \text{ mm}^2$ or $2.5 \times 4 \text{ mm}^2$ and were bonded to PZT with a quick dry epoxy of thickness 1 to 2 μm . The composites were placed in a coplanar waveguide excitation structure. For measurements of the strengths of CME effects, profiles of S_{21} vs f as in Fig.3(a) were recorded for DC voltage $V = -250 \text{ V}$ to $+350 \text{ V}$ applied across PZT.

Studies on CME were done in 3 steps. First, the FMR resonance field H_r was measured as a function of orientation of in-plane magnetic field H (defined by angle ϕ measured from [001] axis) for a constant frequency to identify the principal crystallographic axes. Second, the variation in the resonance frequency f_r with H was measured for H along the principal axes so that magnetic parameters for the NFO film could be estimated from H_r vs ϕ and f_r vs H data. Finally, f_r was measured with a DC voltage V (for $-250 \text{ V} < V < +350 \text{ V}$) applied across PZT for estimation of the E -induced magnetic anisotropy field H_{ME} and the ME coupling constant $A = H_{ME} / E$.

Figure 4(a) shows data on H_r vs ϕ for a composite of PZT and 600 nm thick NFO on (110) MGO. The results are for $f = 12$ GHz and H applied at an angle ϕ measured from the [001] edge of ferrite film. The data in Fig.4(a) is typical of expected variation of H_r with ϕ for NFO on (110) substrates. The data indicate the easy direction to be [1,-1,1] and the hard direction is [001] which is consistent with the M vs H data in Fig.2. Figure 4(b) shows measured f_r vs. H for the field parallel to either [001] or [1,-1,0]. For (110) NFO, the resonance frequency $f_r = f$ is given by

$$f = \gamma \sqrt{(H_0 + 4\pi M_{eff} + \left(-\frac{3}{8} + 2 \cos(2\phi) + \frac{3}{8} \cos(4\phi)\right) \frac{H_4}{2})(H_0 + \left(\frac{1}{2} \cos(2\phi) + \frac{3}{2} \cos(4\phi)\right) \frac{H_4}{2})} \quad (1)$$

In Eq. (1), γ is the gyromagnetic ratio, $4\pi M_{eff} = 4\pi M_s + H_u$ where $4\pi M_s$ is the saturation magnetization and H_u is the growth-induced uniaxial anisotropy, and H_4 is the cubic magneto-crystalline anisotropy field. By fitting the data in Fig.4 to Eq.(1) and assuming $\gamma = 3$ GHz/kOe [28], we obtained the values of the magnetic parameters listed in Table 1 for the NFO film.

Both $4\pi M_s$ and H_4 for the film on (110) MGO are in agreement with reported values for bulk

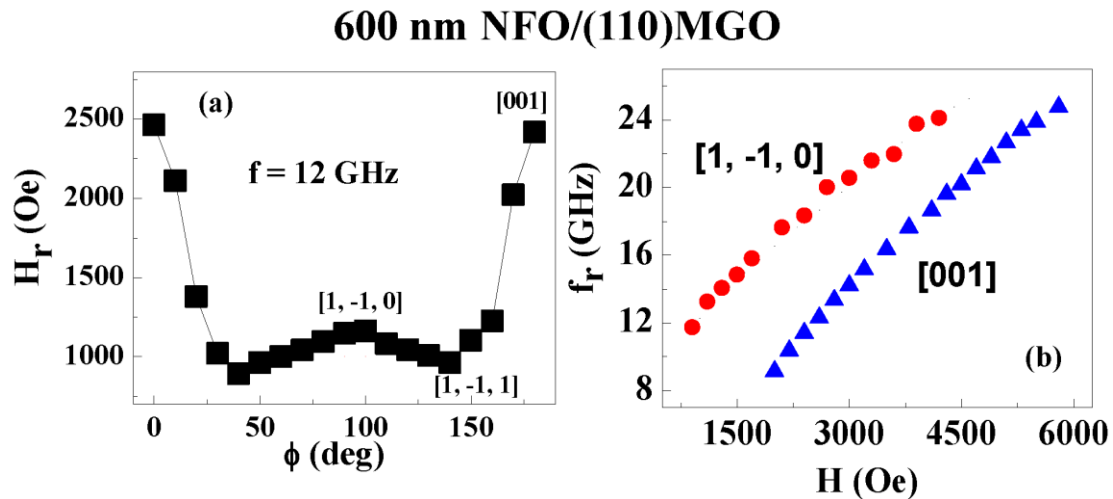


Fig.4. (a) Ferromagnetic resonance (FMR) field H_r as a function of in-plane angle ϕ between [001] and direction of static field H for NFO on (110) MGO. H_r was measured from profiles as in Fig.3(b). (b) FMR frequency f_r vs H data estimated from profiles as in Fig.3(a) for NFO on (110) MGO.

Table 1: Estimated effective saturation magnetization $4\pi M_{eff}$ and cubic magneto-crystalline anisotropy field H_4 for NFO films on MGO and CGO substrates. The growth induced anisotropy field H_u was calculated from $4\pi M_{eff}$ obtained from FMR data as in Fig.4 and saturation magnetization $4\pi M_s$ values from data in Fig.2 and from Ref.28.

System	$4\pi M_{eff}$ (kG)	H_4 (Oe)	$4\pi M_s$ (kG)	H_u (kOe)
600 nm NFO/(110) MGO	8.25	-780	3.5	4.75
600 nm NFO/(100) MGO	13.9	-470	3.5	10.4
450 nm NFO/(100) MGO	11.7	-450	3.5	8.2
1 μ m NFO/(110) CGO	4.5	-300	3.5	1.0
800 nm NFO/(100) CGO	4.7	-400	3.5	1.2

single crystals [29]. The anisotropy field $H_u = 4.75$ kOe is of the easy-plane type with (110) being the easy plane and is smaller than $H_u = 11.9$ kOe reported for NFO on (100) MGO [28].

For studies on CME, profiles of S_{2l} vs f for PZT/NFO/(110) MGO were recorded by applying a DC voltage across the thickness of PZT. Figure 5(a) shows representative data on S_{2l} vs f for H parallel to [001], which is one of edges for the substrate, and for $V = 0, 350$ V and -250 V. The profiles show an up-shift in f_r as the voltage is decreased from +350 V to 0 and then to -250 V. Positive V corresponds to E parallel to the field direction used for poling the PZT. Data on variation of f_r with V obtained from the profiles is shown in Fig.2(b). The resonance frequency f_r increases as V is decreased from + 350 V to zero. For negative V values f_r increases with increasing magnitude of V .

In order to estimate the CME coupling constant A , it is necessary to determine the E -induced anisotropy field $H_{ME} = A E$ using the f_r vs E data in Fig.5 and fitting it to the resonance condition in Eq. (1). For H parallel to [001], $f = f_r$ is obtained by substituting $\phi = 0$ in Eq. (1):

600 nm NFO/(110)MGO: H // [001]

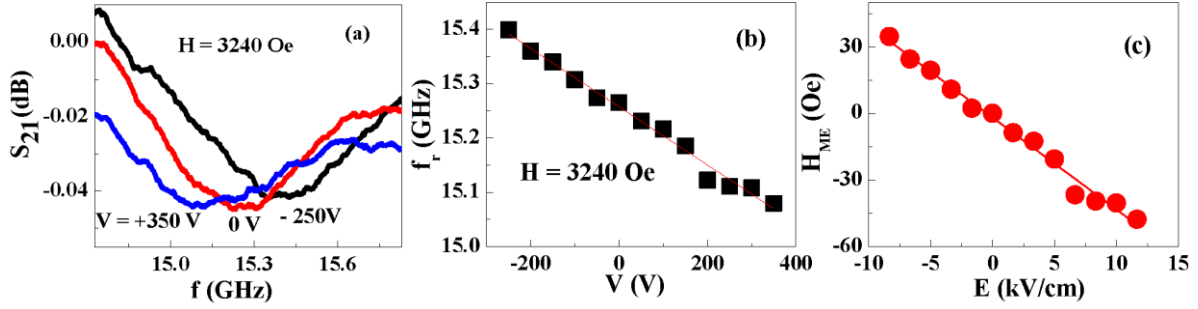


Fig.5. (a) S_{21} vs f profiles showing voltage tuning of FMR for composites of PZT and NFO film on (110) MGO. The data are for H along [001] and for V applied across PZT. (b) f_r as a function of V obtained from FMR profiles as in Fig.5(a). (c) E induced anisotropy field H_{ME} due to CME interaction between NFO and PZT. Data in Fig.5(b) were used to estimate H_{ME} .

$$f = \gamma \sqrt{(H_0 + 4\pi M_{eff} + H_4 + H_{ME})(H_0 + H_4 + H_{ME})} . \quad (2)$$

Figure 5(c) shows H_{ME} estimated using Eq. (2). A linear variation in H_{ME} with E is evident and A determined from linear fit to the data is $A = -4$ Oe cm/kV. The negative sign is associated with decrease in f_r with E seen in the data of Fig.5(b).

Similar FMR measurements under an electric field were performed for H parallel to the two other principal axes, [1,-1,1] and [1,-1,0]. H_{ME} was then estimated using the following expressions for $f = f_r$. For H along [1,-1,1] axis $\phi = 54^\circ$ and f is given by

$$f = \gamma \sqrt{(H_0 + 4\pi M_{eff} - 0.64 H_4 + H_{ME})(H_0 - 0.68 H_4 + H_{ME})} \quad (3).$$

For H parallel to [1,-1,0] axis $\phi = 90^\circ$ and one obtains

$$f = \gamma \sqrt{(H_0 + 4\pi M_{eff} - H_4 + H_{ME})(H_0 + 0.5 H_4 + H_{ME})} . \quad (4)$$

Figure 6 shows H_{ME} vs E for these two H orientations and the estimated A -values are given in Table 2. Thus for composites with NFO films on (110) MGO, $A = 5.6$ Oe cm/kV is the highest for $H // [1,-1,0]$ and $A = 2.8$ Oe cm/kV is the lowest for $H // [1,-1,1]$.

600 nm NFO/(110)MGO

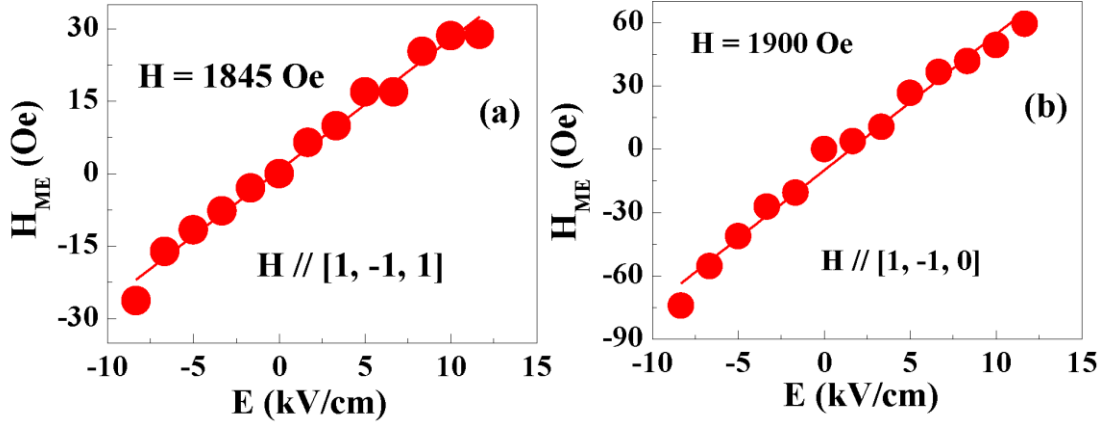


Fig.6. Results on (a) H_{ME} vs E as in Fig.5 for H along $[1,-1,1]$ for composites of PZT and NFO on (110) MGO. (b) Similar H_{ME} vs E for H along $[1,-1,0]$.

Table 2: The average converse ME coupling coefficient A determined from FMR under a static electric field for composites of PZT and NFO films on (110) and (100) MGO.

Ferrite thickness	substrate	H orientation	A (Oe cm/kV)
600 nm	(110)MGO	[001]	-4.0
		[1, -1, 1]	2.8
		[1, -1, 0]	5.6
600 nm	(100)MGO	[001]	4.6
		[011]	2.5

3.2. Composites of PZT and NFO films on (100) MGO substrates

Similar studies on CME were carried out on composites with 600 nm and 450 nm NFO films deposited on (100) MGO substrates. Figure 7(a) shows the dependence of H_r on angle ϕ measured from [001] axis of 600 nm NFO film for an excitation frequency of 13 GHz. The variation in H_r with ϕ is typical of (100) spinel ferrites and the data indicate [011] to be the easy axis and [001] is the hard axis. Variation in f_r with H for the two principal axes are shown in Fig.7(b) and fitted to the resonance condition:

$$f = \gamma \sqrt{(H_0 + 4\pi M_{eff} + (\frac{3}{4} + \frac{1}{4} \cos(4\phi)) H_4)(H_0 + H_4 \cos(4\phi))}. \quad (5)$$

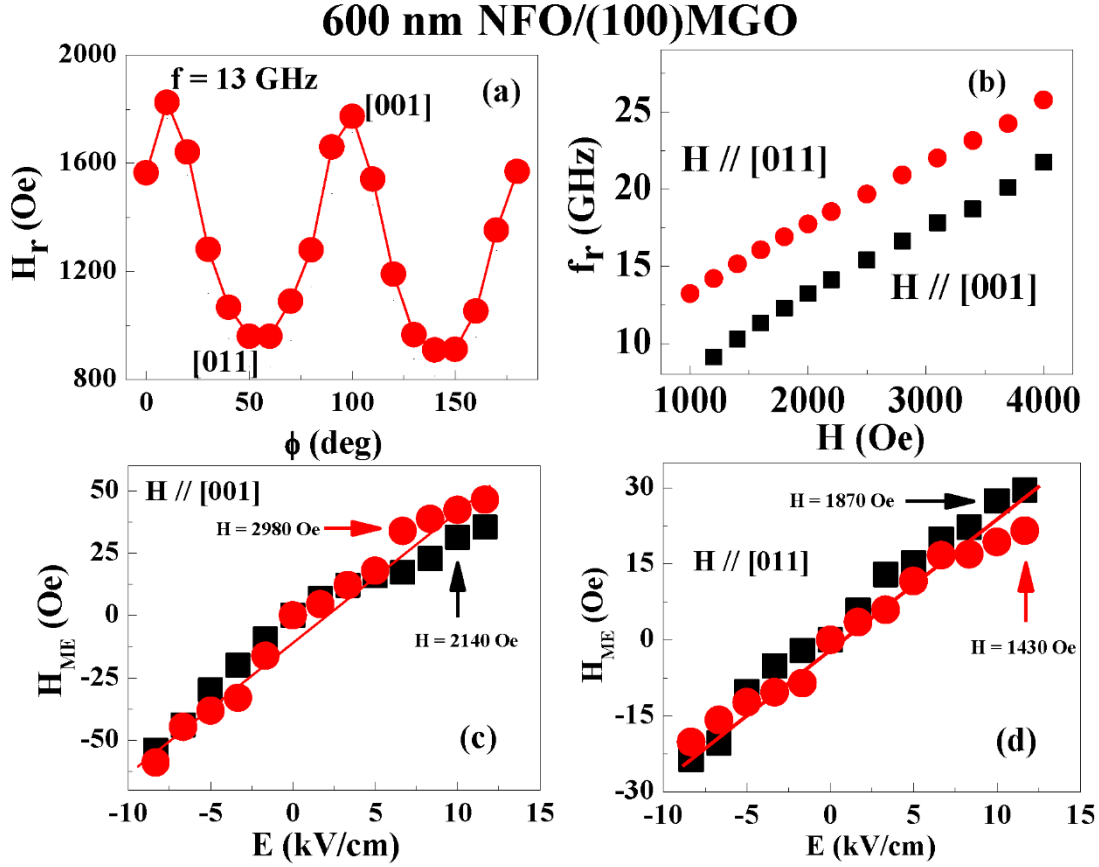


Fig.7. (a) Resonance field H_r as a function of in-plane angle ϕ for direction of H measured from $[001]$ axis for 600 nm NFO film on (100) MGO. (b) Resonance frequency f_r vs H for NFO on (100) MGO. (c) Estimated H_{ME} as a function of E for composites of PZT and NFO on (100) MGO for representative H -values = 2140 Oe and 2980 Oe along $[001]$. (d) H_{ME} vs E for $H = 1430$ Oe and 1870 Oe along $[011]$ axis for NFO film on (100) MGO substrate and PZT.

Estimated magnetic parameters for the ferrite film from data in Figs.7 (a) and (b) are given in Table 1. The cubic anisotropy field H_4 for the film is smaller than for the film on (110) MGO, but the in-plane uniaxial anisotropy field $H_u = 10.4$ kOe is more than twice the value for the 600 nm NFO film on (110) MGO.

Ferromagnetic resonance profiles under an electric field were then obtained for a series of H -values parallel to $[001]$ and $[011]$ and H_{ME} -values were estimated by fitting the f_r vs E data to the following equation for FMR frequency $f_r = f$:

For $H//[001]$: $\phi = 0$ and

$$f = \gamma \sqrt{(H_0 + 4\pi M_{eff} + H_4 + H_{ME})(H_0 + H_4 + H_{ME})} \quad (6)$$

For $H//[011]$: $\phi = 45^\circ$ and

$$f = \gamma \sqrt{(H_0 + 4\pi M_{eff} + 0.5H_4 + H_{ME})(H_0 - H_4 + H_{ME})} \quad (7)$$

Figures 7(c) and (d) show the variation in H_{ME} with E for H along [001] and [011], respectively, and the corresponding A -values are given in Table 2. For $H // [001]$, A is positive and its magnitude is comparable to magnitude of A for $H// [001]$ for NFO on (110) MGO, whereas $A = 2.45$ Oe cm/kV for $H // [011]$ is a factor of two smaller than the A -value for $H // [1,-1,0]$ for the film on (110) MGO.

Similar measurements on composites with 450 nm NFO on (100) MGO yielded A -values of 4.1 – 4.3 Oe cm/kV for $H//[001]$, in agreement with values in Table 2 for the composite with 600 nm NFO.

3.3. Composites of PZT and NFO on (110) and (100) CGO substrates

Films of NFO on CGO substrates were also used in composites with PZT for studies on CME effects. Ferrite films of thickness 1 μm on (110) on CGO were first characterized by FMR. Figure 8(a) shows the dependence of H_r on direction of H measured from [001] axis. It is evident from the data that [1,-1,1] is the easy axis and [1,-1,0] is the hard axis. The magnetic parameters $4\pi M_{eff}$, anisotropy field H_4 and $4\pi M_s$ determined from FMR and static magnetization M vs H (Fig.2) are given in Table 1. The in-plane growth induced anisotropy field $H_u \sim 1$ kOe is small compared to 4.75 kOe for films on (110) MGO. The relatively small H_u can be attributed to smaller film-lattice mismatch of 0.2% in the case of films on CGO versus 0.8% for NFO on (110) MGO.

Studies on CME were done on composites of PZT and NFO films on (110) CGO. Figures 8(b)-(d) show the E dependence of H_{ME} obtained from f_r vs E data and Eqs.(2)-(4) for H along

the three principal axes. For $H//[001]$ we observed a decrease in FMR frequency f_r with E , similar to the data in Fig.5(b) for composite with NFO on (110) MGO. The anisotropy field H_{ME} is therefore negative for $+E$ values and the ME coefficient A is negative. For H -along the other two principal axes, however, H_{ME} is positive for $+E$ with a linear increase in its magnitude with increasing E and the A -values are given in Table 3. The strength of CME effect is the highest for $H // [1,-1,0]$.

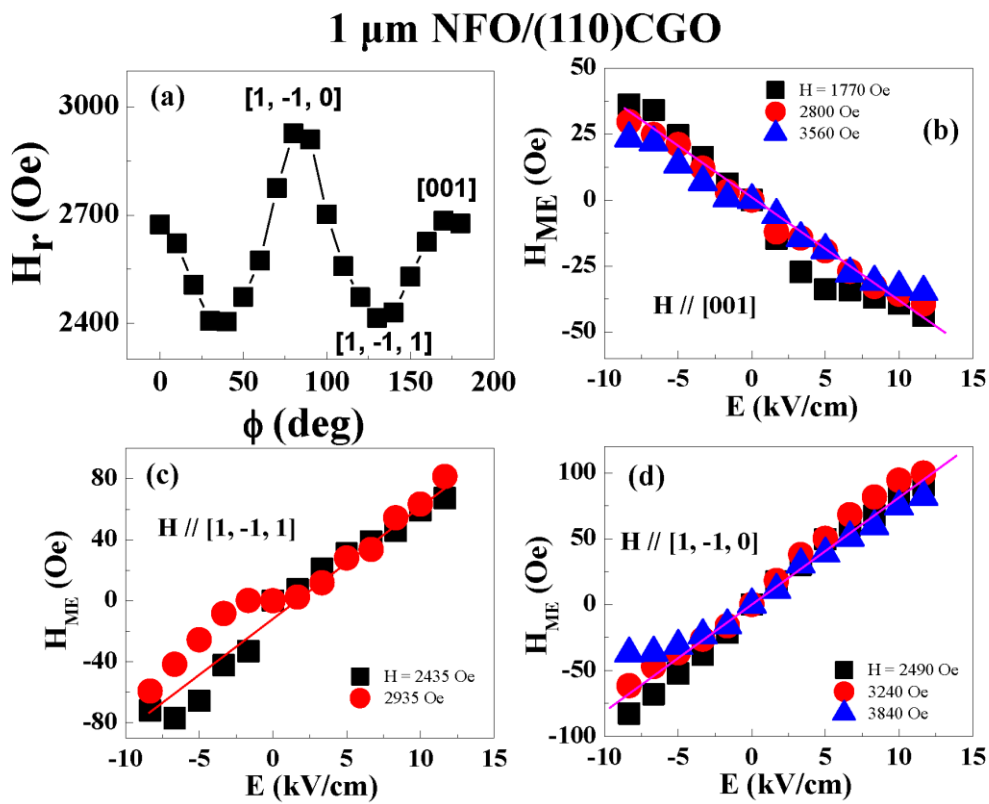


Fig.8. (a) Variation of resonance field H_r with the angle ϕ for direction of H measured from $[001]$ axis for $1 \mu\text{m}$ thick NFO film on (110) CoGa_2O_4 (CGO) substrate. The frequency was 13 GHz. Estimated H_{ME} vs E for a series of static magnetic fields H along (b) $[001]$, (c) $[1,-1,1]$ and (d) $[1,-1,0]$ direction for composites of NFO on (110) CGO and PZT.

Finally, we carried out studies on CME in composites of PZT with 800 nm NFO film on (100) CGO substrate. Magnetic parameters for the film determined from magnetization and FMR data are provided in Table 1. The anisotropy fields H_4 and H_u are approximately the same

as for the film on (110) CGO. Data on FMR under E were recorded for $H//[001]$ and H along the diagonal of the rectangular sample of NFO that corresponded to in-plane angle $\phi = 31^\circ$.

Table 3: The average converse ME coupling coefficient A determined from FMR under a static electric field for composites of PZT and NFO films on (110) and (100) CGO substrates.

Ferrite thickness	substrate	H orientation	A (Oe cm/kV)
1 μm	(110)CGO	[001]	-3.8
		[1, -1, 1]	6.8
		[1, -1, 0]	8.1
800 nm	(100)CGO	[001]	5.2
		$\phi = 31^\circ$	3.0

Figure 9 shows H_{ME} vs E for both cases and the ME coefficient A are given in Table 3. The coefficient A for H along [001] axis is comparable to A -values for H along [001] for ferrite films on (110) CGO.

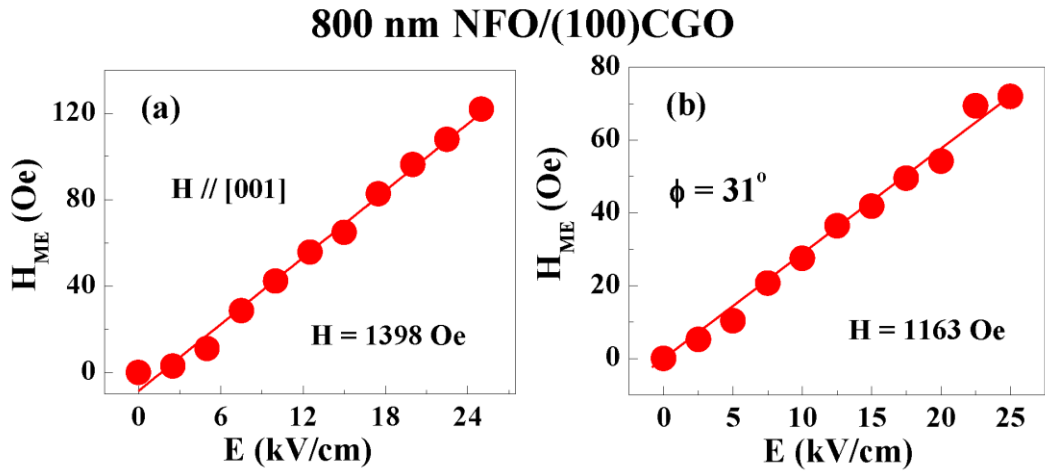


Fig.9. H_{ME} obtained from data on FMR under an electric field E for composites of PZT and 800 nm thick NFO film on (100) CGO for H along (a) [001] and (b) along the diagonal of the rectangular sample, at angle of 31° from [001] axis.

4. Theory

We consider next a model for the CME in the composites. Past efforts in this regard were primarily on ferrite-ferroelectric composites [30,31]. In a composite of NFO/PZT an applied E -field across the PZT layer generates an in-plane, compressive strain $\Delta L/L = E d$. The

transfer of this strain to NFO will produce a stress $\sigma = E d Y/(1-\nu)$, where Y is the Young's modulus and ν is the Poisson's ratio for NFO. The stress will manifest as an induced anisotropy field H_{ME} and the ME coefficient $A = H_{ME}/E = 3 \sigma \lambda/(E M_s) = 3 Y \lambda d/(1-\nu) M_s$ [23]. It is, however, necessary to consider in a formal model the influence of parameters such as the volume of ferroic phases and any non-ferroic substrates that will not have any contribution to ME coupling. A detailed theory predicted $A = 2$ Oe cm/kV for a layered NFO-PZT composite with volume fractions of 50% NFO and 50% PZT [30].

There are several features in the results of the present study that cannot be explained based on the past models. These features include the following. (i) Negative A -value for $H \parallel [001]$ for NFO films on (110) MGO or CGO substrates (Figs. 5 and 8) and is due to a *decrease* in f_r with increasing magnitude of $+E$. (ii) H -orientation dependence of A for composites with NFO on (100) substrates. Such a dependence is not anticipated based on past models. A key drawback in the past models was bending deformation expected in an asymmetric ferromagnetic-ferroelectric composites under an applied E - or H -field was not considered. Such a bending under E -field in this present case will result in both compressive and tensile strains as illustrated in Fig.10, leading to the features in A mentioned above.

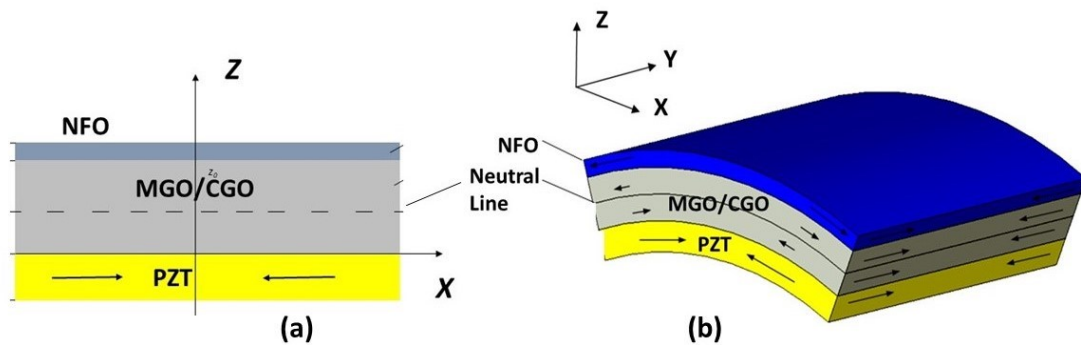


Fig.10. Schematic diagram showing (a) composites of PZT and NFO film on MGO or CGO substrate and (b) compressive and bending deformations and the neutral plane. The arrows indicate the compressive and tensile strain in the composite.

In the case of composites of PZT and NFO on (110) substrates and for E along the Z-axis, the relative strengths of elastic stiffness constants prefer compressive deformation along the Y-axis ([1,-1,0] direction) and bending along the X-axis ([001] direction). This bending leads to tensile strain of the NFO film along [001] direction and, due to the Poisson effect, compression along [1,-1,0] direction. For the composites with NFO on (100) substrates, the directions [001] and [010] are equivalent. But the magnetic field applied along one axis breaks this symmetry and H along the [001] direction leads to compressive strain $\lambda(H)$ along this axis and tensile strain along [010] direction. Upon the application of E , piezoelectric strain will give rise to bending along [010] (X axis in Fig.10 b) and compressive strain along [001] direction (Y axis in Fig. 10 b).

A comprehensive theory for the ME effect is discussed in the Appendix. Expressions for CME coupling constant A were obtained as a function of H orientation for composites of PZT and NFO film on MGO. We assumed material parameters for bulk polycrystalline or single crystals of PZT, MGO and NFO [32-34] and estimated A -values given below.

For composites of PZT/NFO/(110)MGO:

$$A_{[001]}^{(110)} = -3.95 \text{ Oe} \cdot \text{cm} / \text{kV} \quad A_{[1-10]}^{(110)} = 5.64 \text{ Oe} \cdot \text{cm} / \text{kV} \quad , \text{ and } A_{[1-11]}^{(110)} = 2.82 \text{ Oe} \cdot \text{cm} / \text{kV} .$$

For PZT/NFO/(100) MGO:

$$A_{[100]}^{(100)} = 2.24 \text{ Oe} \cdot \text{cm} / \text{kV} , \quad A_{31}^{(100)} = 1.16 \text{ Oe} \cdot \text{cm} / \text{kV} . \quad A_{[110]}^{(100)} = 0.67 \text{ Oe} \cdot \text{cm} / \text{kV} \quad .$$

Significant findings from the model are as follows. For the composite with (110) films (i) the theory predicts a negative value for the ME constant A for H along the [001] direction and positive value for $H // [1,-1,0]$ and $[1,-1,1]$ directions, which are consistent with the

measurements. (ii) The numerical values of A are in very good agreement with the experimental values for PZT/NFO/(110) MGO in Table 2. (iii) The highest A -value is estimated for $H // [1,-1,0]$ direction and is a factor two higher than ME constant for H along $[1,-1,1]$ direction. For composite with NFO on (100) MGO substrates (i) the highest A -value is estimated for $H // [001]$ and (ii) as H orientation angle ϕ measured from $[001]$ is increased A is predicted to decrease and is estimated to be minimum for H along $[011]$. The measured values in Table 2 for PZT/NFO/(100) MGO, however, are higher than the estimated values. Similar theoretical values for composites on CGO substrates could not be done due to lack of available data on material parameters for CGO substrates.

5. Discussion

Here we discuss results on magnetic and ME characterization of NFO films and composites with PZT. The ME coefficient A in the composites are then compared with measured values in similar ferromagnetic and ferroelectric composites. Nickel ferrite films of thickness 450 nm to 1 μm deposited by PLD techniques on MGO or CGO were found to have magnetization, FMR line-width ΔH and cubic anisotropy field values in agreement with reported values for bulk single crystals. The preferred orientation for magnetization was in-plane for films on both substrates with growth induced anisotropy field $H_u \sim 1-1.2$ kOe for films on CGO and 4.75 – 10.4 kOe for films on MGO. The single-crystal like FMR profiles with small ΔH for the films facilitated studies on CME effects in composites with polycrystalline PZT. In composites with films on (110) substrates, it was possible to investigate the influence of orientation of H along the three principal axes, $[001]$, $[1,-1,0]$ and $[1,-1,1]$, (and therefore the corresponding magnetostriction) on the strength of CME whereas for films on (100) substrates

studies were done for H along either [001] or [011].

For the composite with NFO film on (110) MGO both the sign and magnitude of the coefficient A in Table 2 are well accounted for by our model with the strongest coupling for H along [1,-1,0] and the weakest for $H // [1,-1,1]$. This is in agreement with the expectation of the weakest coupling for H along [1,-1,1] due low magnetostriction compared to the other two principal axes [29,35]. Another significant and first such observation is the negative A -value for $H // [100]$, leading to a decrease in the resonance frequency f_r with the application of an E -field in the same direction as the initial poling field applied to PZT. A negative shift in f_r is generally seen in composites with PZT only when the polarity of E is reversed and is due to switch in the piezoelectric strain from compressive to tensile or vice versa [23]. For composites of PZT and NFO on (100) MGO, however, A -value of 4.6 Oe cm/kV is positive for $H//[001]$. The magnitude of A for $H//[001]$ is approximately equal for composites with NFO films on either (100) or (110) MGO. The weakest CME coupling is measured for $H//[011]$ for samples with NFO on (100) MGO.

The overall strength of the converse ME effect for composites with NFO on CGO substrates (Table 3) is higher than for samples with MGO substrates. This cannot be attributed to larger NFO film thickness of 0.8 to 1 μm on CGO compared to 0.45 to 0.6 μm for films on MGO. For a given PZT thickness, one would in fact expect a weaker mechanical deformation and a decrease in A -value when the thickness of the ferrite film is increased. The strong ME coupling for composites with CGO will then have to understood in terms of a relatively small film-lattice mismatch compared to MGO. The in-plane compressive stress due to this mismatch and the resulting magnetic anisotropy field is almost a factor of five

smaller for CGO than for MGO [28]. Thus one has to infer that the CGO substrate seems to allow for efficient transfer of piezoelectric strain in PZT to the ferrite film and also a large magnetostrictive deformation in NFO films due to weak substrate clamping. For the composite with NFO/(110) CGO the A -value for $H // [001]$ is negative, in agreement with the sign and magnitude of A for samples with (110) MGO. The highest A -value amongst the systems studied is measured for H along $[1,-1,0]$ for NFO/(110) CGO.

It is essential to compare the CME coupling strength in the present system with results for similar composites. The nature of CME has been investigated in several multiferroic composites consisting of ferroelectric PZT, barium titanate (BTO), PMN-PT or lead zinc niobate-lead titanate (PZN-PT) and ferromagnetic metals/alloys, YIG, spinel ferrites or hexagonal ferrites [23]. Composites were made by a variety of techniques including epoxy or eutectic bonded thick film structures and thin film heterostructures by spin-spray coating, PLD, and chemical vapor deposition (CVD). Measurements involved either M vs H or FMR under a static electric field.

Systems studied so far could be classified into two categories: (i) Layered thick film or thin film composites of ferromagnets either bonded or deposited onto ferroelectrics and (ii) Ferroelectrics and ferromagnetic films on non-ferroic substrates. In the first case the strength of CME coupling depends on the volume/thickness ratio of the ferromagnetic-to-ferroelectric phase with A -value increasing with decreasing thickness of the ferromagnetic layer [30]. In the case of composites with non-ferroic substrates the strain transfer between the ferroic layers is weakened by the substrate and ME coupling is also generally weak.

Amongst the ferromagnetic-ferroelectric composites without any non-ferroic substrates

the highest A -values were reported for ferromagnetic thin films such as FeGaB deposited on PZT, PMN-PT or PZN-PT [38-40]. Thin films of FeGaB on PMN-PT showed $H_{ME} = 330$ Oe for $E = 8$ kV/cm, corresponding to $A \sim 40$ Oe cm/kV [40]. Films of Fe₃O₄ prepared by spin-spray on ferroelectrics showed strong CME with A values as high as 108 Oe cm/kV [41]. In spite of very high A -values, the FMR linewidths for FeGaB or Fe₃O₄ that range from 300 to 800 Oe are too high for practical devices. Among the composites with low-loss ferromagnets, epoxy bonded PZT and single crystal M-type barium hexaferrite, BaM, and barium-aluminum hexaferrites showed very weak CME with $A \sim 0.2$ Oe cm/kV [42,43] and the highest A -value of 3 Oe cm/kV for hexaferrite-ferroelectric system was reported for composites of Y-type hexaferrite/PMN-PT [44].

A system of particular interest to the present study is NFO films deposited onto ferroelectric PMN-PT and PZN-PT by CVD techniques [45]. For 1.5-2 μm thick NFO on 0.5 mm thick PMN-PT the measured A -value of 16 Oe cm/kV is almost a factor of 2-4 higher than A -values for the present systems due to (i) thick piezoelectric layer, 0.5 mm vs 0.2-0.3 mm for the present systems, and an order of magnitude higher piezoelectric coefficient d for PMN-PT than for PZT and (ii) absence of a non-ferroic substrate such as MGO or CGO that dissipate the E -induced piezoelectric strain and weakens the ME coupling. The NFO/PMN-PT composite, however, is not suitable for use in microwave devices due to very high $\Delta H \sim 670$ Oe for NFO [45].

Early works on CME on composites with non-ferroic substrates were on YIG on gadolinium gallium garnet (GGG) substrates-PZT and YIG/GGG-PMN-PT since YIG is one of the preferred material for microwave devices [23,36,37]. But the A -values for composites

with YIG were rather small, on the order of 1 Oe cm/kV due to very low magnetostriction for YIG [25,36]. The average CME coupling coefficients in Tables 2 and 3 are much higher than for composites of YIG films on GGG and PZT or PMN-PT.

Results of the present study in Figs.4-9, Tables 2 and 3, the additional data on FMR profiles and A -values as a function of bias field H - in the supplemental information [Ref.46] and the theory provide a viable and promising path for the realization of voltage tunable nickel ferrite-ferroelectric composite based devices. The key ingredients for such devices are (i) low FMR line width for the ferromagnet, (ii) ferroelectrics with high piezoelectric coefficient and (iii) either total elimination or a reduction in the thickness of non-ferroic substrate. It is clear from our previous studies on NFO films on PMN-PT that NFO deposited by CVD techniques showed a high ΔH -value and the ubiquitous presence of antiphase boundaries in epitaxial ferrite thin films degrades their magnetic and microwave characteristics as compared to bulk single crystal counterparts that make them unacceptable for device applications [45]. It is also evident from this study that by using MGO or CGO substrates that have similar crystallographic structure and small lattice mismatch with NFO, it is possible to grow films without any antiphase boundaries. Consequently, these films show dramatically improved magnetic and loss parameters comparable with bulk single crystals. Another key finding of this study is the large in-plane growth induced anisotropy in NFO that will either eliminate or reduce the bias magnetic field necessary for the devices. The low FMR line-width, in combination with a large in-plane growth induced anisotropy field make these composites ideal for use in self-biased devices that could function without the need for an external bias magnetic field, a feature that is suitable for device miniaturization and integration with semiconductor

devices. Finally, a significant enhancement in A and broad-band tunability of such devices can be achieved by reduction of substrate thickness.

6. Conclusions

In conclusion, epitaxial NFO films of thickness 450 nm to 1 μm were grown by PLD on (110) and (100) MgGa_2O_4 and CoGa_2O_4 , substrates. Characterization by magnetization and FMR revealed an easy-plane growth induced anisotropy H_u ranging from a minimum of 1 kOe for NFO on (110) CGO to a maximum of 10.4 kOe for NFO on (100) MGO, with the films on MGO having a much higher H_u than the NFO on CGO. The FMR line-widths for the ferrite films were in the range 25 to 50 Oe and were used for investigations on the converse ME effects in epoxy bonded composites with polycrystalline PZT. The studies were aimed at the influence of orientation of the bias magnetic field H on the ME coupling constant A . Data on E -tuning of FMR were obtained for H parallel to the principal crystallographic axes of NFO films on (110) and (100) substrates and were used to estimate the induced anisotropy field H_{ME} due to ME interactions. A linear variation of H_{ME} with E was evident from the data and the ME constants $A = H_{ME}/E$ were determined. For composites with (110) films, A was found to be negative for H along [001] and positive for $H // [1,-1,0]$ and $[1,-1,1]$ with the strongest coupling measured for H along $[1,-1,0]$. For (100) films, A was found to be higher for H along [001] than for $H // [011]$. Composites with films on CGO showed a stronger ME coupling than for films on MGO. A model was developed the converse ME effects and estimated A -values were found to be in good agreement with the measured values.

Acknowledgements

The research at Oakland University was supported by grants from the National Science Foundation (ECCS-1307714, DMR-1808892), while work at the University of Alabama was supported by NSF Grant No. ECCS-1509875. The efforts at Hubei University was supported by the National Science Foundation of China (Grant Nos. 51372074, 51472078). The research at AFRL was supported by the Air Force Office of Scientific Research under project number FA9550-15RXCOR198 and a Summer Faculty Fellowship for G.S. The authors are grateful to Dr. Zbigniew Galazka of the Leibniz Institute for Crystal Growth, Berlin, Germany, for providing the MGO and CGO crystals from which the substrates were fabricated.

Appendix - Theory

A model for the converse ME effects in the composites is discussed in this section. The influence of an external static electric field E upon a magnetic resonance spectrum can be described by means of an additional term in the magnetic free energy. For the cubic crystals this term is represented in a rectangular coordinate system $(1,2,3)$ by [30]:

$$F_{me} = B_1(S_1\alpha_1^2 + S_2\alpha_2^2 + S_3\alpha_3^2) + B_2(S_6\alpha_1\alpha_2 + S_5\alpha_1\alpha_3 + S_4\alpha_2\alpha_3), \quad (8)$$

where B_1 and B_2 are the magnetostrictive constants, α_i are the direction cosines of the magnetization M , S_i are the components of the strain tensor. The magnetostrictive constants can be determined through the magnetostriction coefficients λ_{100} and λ_{111} and the elastic modules c_{11} , c_{44} as $\lambda_{100} = -\frac{2}{3} \frac{B_1}{c_{11} - c_{12}}$, $\lambda_{111} = -\frac{1}{3} \frac{B_2}{c_{44}}$. The induced magneto-electric

anisotropy field H_{ME} has the following expression:

$$H_{me} = \frac{3^m Y}{M_s (1 + \nu)} \left[\lambda_{100} \cdot (S_1 \alpha_1^2 + S_2 \alpha_2^2 + S_3 \alpha_3^2) + \lambda_{111} (S_6 \alpha_1 \alpha_2 + S_5 \alpha_1 \alpha_3 + S_4 \alpha_2 \alpha_3) \right], \quad (9)$$

where M_s is saturation magnetization, ${}^m Y = (c_{11} - c_{12})(1 + \nu)$ and ${}^m G = c_{44}$ are the Young's modulus and shear modulus, respectively. The components of the strain tensor S_i can be determined by solving system of elastic equations for the magnetic film, piezoelectric layer and substrate.

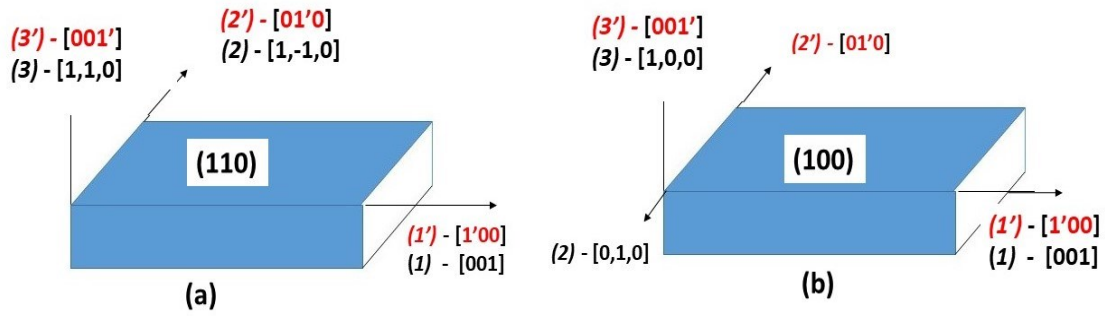


Fig.11. Schematic diagram showing the composite, the sample coordinate system ($1' 2' 3'$), and the crystallography coordinate system (123) for (a) ferrite films on (110) substrate and (b) ferrite film on (100) substrate.

Consider the composite structures with NFO films on (110) or (100) substrates and the “sample” coordinate system ($1' 2' 3'$) and crystallographic coordinate system (123) in Fig. 11. Electric field applied along the polarization direction results in in-plane strain in the piezoelectric. This leads to the development of off-center longitudinal force acting on the system. Two types of deformation arise under the action of this force - off-center longitudinal bending along one axis and compressive deformation along the other axis. The bending must occur along the axis that has the lowest bending stiffness. Depending on the conditions, this may be the $1'$ axis or the $2'$ axis. Bending along the axis creates a stiffer edge, therefore simultaneous bending with respect to axes $1'$ and $2'$ under the action of longitudinal forces is

difficult to realize. Thus, compressions in piezoelectric phase along axis $1'$ and axis $2'$ lead to bending of the sample along one axis in-plane and compression along second axis in-plane and also compression along the axis out-of-plane. For determination of the strain components caused by compression we use the system of elastic equations (Hooke's law) in the following form:

$$\begin{cases} {}^p S_{i'} = \frac{1}{{}^p Y} ({}^p \sigma_{i'} - \nu {}^p \sigma_{j'}) + d_{3'i'} E_{3'}, \\ {}^s S_{i'} = \frac{1}{{}^s Y'} ({}^s \sigma_{i'} - \nu {}^s \sigma_{j'}) , \\ {}^m S_{i'} = \frac{1}{{}^m Y'} ({}^m \sigma_{i'} - \nu {}^m \sigma_{j'}) + \lambda_{i'}(H). \end{cases} , \quad (10)$$

where $i' = 1, j' = 2$ or vice versa $i' = 2, j' = 1$, ν is the Poisson's ratio, $\lambda_{i'}(H)$ is magnetostriction along i' direction. Using the assumptions ${}^p u_{i'} = {}^s u_{i'} = {}^m u_{i'} = u_{i'}$ and the equilibrium conditions ${}^m \sigma_{i'} {}^m t + {}^s \sigma_{i'} {}^s t + {}^p \sigma_{i'} {}^p t = 0$ we get for the nonzero strain component, caused by compression along i' axis, the following expressions:

$$\begin{aligned} {}^m S_{c,i'} &= \left(\frac{{}^p Y {}^p t}{{}^p \bar{Y} t} d_{3'1'} E_{3'} + \frac{{}^m Y {}^m t}{{}^m \bar{Y} t} \lambda_{i'}(H) \right) , \\ {}^m S_{c,3'} &= -\nu ({}^m S_{c,1'} + {}^m S_{c,2'}) \end{aligned} \quad (11)$$

where $\bar{Y} = \frac{({}^p Y {}^p t + {}^s Y {}^s t + {}^m Y {}^m t)}{t}$ is the average value of Young's modulus for the composite,

$t = ({}^p t + {}^s t + {}^m t)$ is the total thickness of the composite structure and for PZT $d_{3'2'} = d_{3'1'} = d_{31}$.

For determination of the strain components caused by bending we use the coordinate system (X, Y, Z) with axis X along the axis of bend (axis $1'$ or axis $2'$). The cross section of the sample to determine the bending deformations is shown in Fig. 10.

For determination of the strain components from bending we use a modified method of the strength of material [31]. Using the Bernoulli hypothesis for Z - coordinate of neutral line

we obtain the following expression

$$z_0 = \frac{1}{2} \frac{{}^s Y {}^s t^2 + {}^m Y {}^m t^2 + 2 {}^m Y {}^s t {}^m t - {}^p Y {}^p t^2}{{}^s Y {}^s t + {}^m Y {}^m t + {}^p Y {}^p t}, \quad (12)$$

where ${}^p Y$, ${}^p t$, ${}^s Y$, ${}^s t$, ${}^m Y$, ${}^m t$ are Young's modulus and thickness of piezoelectric layer, substrate and ferrite film, respectively. The strain component along X axis S_x is given by the relation

$$S_x = (z - z_0) / \rho, \quad (13)$$

where ρ is the radius of cylindrical plane. This radius related to the bending moment and geometrical characteristics of the cross section by expression

$$1 / \rho = M / D, \quad (14)$$

where effective bending stiffness $D = {}^p Y {}^p J_{y_0} + {}^s Y {}^s J_{y_0} + {}^m Y {}^m J_{y_0}$. Here ${}^p J_{y_0}$, ${}^s J_{y_0}$, ${}^m J_{y_0}$ are the moment of inertia of the cross section respect to neutral line. We assume that the bending deflection is much less than the thickness of the piezoelectric and the substrate plates. With this approximation the bending moment, produced by applied electric field, is given by the following expression:

$$M = -Y^p d_{31} E_3 W t^p (z_0 + t^p / 2) \quad (15)$$

where W is a width of the sample. Since the ferrite film is thin, we can neglect the change in the deformation of the ferrite through the thickness of the film. In this case we can rewrite Eq. (13) in the form

$${}^m S_x = ({}^s t + {}^m t - z_0) / \rho \quad (16)$$

Using Eq. (14) and Eq. (15) we obtain the following expressions for strain components in NFO film caused by bending

$$\begin{aligned}
{}^m S_{b,1'} &= -d_{31} E_3 \frac{{}^p Y W t^p (z_0 + t^p / 2) ({}^s t + {}^m t - z_0)}{D}, \\
{}^m S_{b,2'} &= {}^m S_{b,3'} = \nu d_{31} E_3 \frac{{}^p Y W t^p (z_0 + t^p / 2) ({}^s t + {}^m t - z_0)}{D}.
\end{aligned} \tag{17}$$

(i) Composites of PZT and NFO film on (110) substrate

For a given sample orientation, the effective bending stiffness $D_{2'} > D_{1'}$, as a result, compression deformations in a piezoelectric material induced by electric field along 3' axis, causes bending along the 1' axis ([001] direction) and compression deformation along the 2' axis ([1-10] direction). The bending along 1' axis leads to tensile strain of the NFO film along this axis and, due to the Poisson effect, to compression along axis 2'. Thus, for a given sample orientation, we have

$$\begin{aligned}
{}^m S_{1'} &= -d_{31} E_3 \left(\frac{{}^p Y W t^p (z_0 + t^p / 2) ({}^s t + {}^m t - z_0)}{D} + \nu \frac{{}^p Y^p t}{\bar{Y} t} \right), \\
{}^m S_{2'} &= d_{31} E_3 \left(\nu \frac{{}^p Y W t^p (z_0 + t^p / 2) ({}^s t + {}^m t - z_0)}{D} + \frac{{}^p Y^p t}{\bar{Y} t} \right).
\end{aligned} \tag{18}$$

For further calculations, it is convenient to write Eq. (18) in the crystallographic coordinate system (123), as shown in Fig.11 (a), using the relations $x_i = \beta_{ik} x_{k'}$, $S_{ij} = \beta_{ik} \beta_{jl} S_{k'l'}$, where $\hat{\beta}$ is the cosines matrix. Using these relations, we get for the strain components the following expressions:

$$S_3 = S_{1'}, \quad S_1 = S_2 = \frac{1}{2}(S_{2'} + S_{3'}), \quad S_6 = \frac{1}{2}(-S_{2'} + S_{3'}), \quad S_4 = S_5 = 0. \tag{19}$$

Thus, substituting these expressions into Eq. (9) for H along [001] direction ($\alpha_1 = \alpha_2 = 0, \alpha_3 = 1$) for magnetoelectric constant A , we get

$$A_{[001]}^{(110)} = -\frac{3^m Y d_{31}}{M_s (1 + \nu)} \lambda_{100} \left[\frac{{}^p Y W t^p (z_0 + t^p / 2) ({}^s t + {}^m t - z_0)}{D} + \nu \frac{{}^p Y^p t}{\bar{Y} t} \right]. \tag{20}$$

For H along [1,-1, 0] direction we have $\alpha_1 = \frac{\sqrt{2}}{2}, \alpha_2 = -\frac{\sqrt{2}}{2}; \alpha_3 = 0$. By substituting these

values into Eq.(9) we obtain

$$A_{[1\bar{1}0]}^{(110)} = \frac{3^m Y d_{31}}{M_s (1+\nu)} \left[\lambda_{100} 2\nu \frac{{}^p Y W t^p (z_0 + t^p / 2) ({}^s t + {}^m t - z_0)}{D} + (\lambda_{100} (1-\nu) + \lambda_{111} (1+\nu)) \frac{{}^p Y^p t}{\bar{Y} t} \right], \quad (21)$$

For the H along $[1,-1,1]$ direction $\alpha_1 = \frac{\sqrt{3}}{3}, \alpha_2 = -\frac{\sqrt{3}}{3}, \alpha_3 = \frac{\sqrt{3}}{3}$. Substituting these values into

Eq. (9) we get

$$A_{[1\bar{1}1]}^{(110)} = \frac{{}^m Y d_{31}}{M_s (1+\nu)} \left[\lambda_{100} (4\nu - 1) \frac{{}^p Y W t^p (z_0 + t^p / 2) ({}^s t + {}^m t - z_0)}{D} + (\lambda_{100} (1-\nu) + \lambda_{111} (1+\nu)) \frac{{}^p Y^p t}{\bar{Y} t} \right]. \quad (22)$$

(ii) Composites of PZT and NFO film on (100) substrate

For the sample with NFO film on (100) substrates the directions $[001]$ and $[010]$ are equivalent, therefore the bending or compression can be evaluated along one and will be the same along the other direction. But the magnetic field applied along one axis breaks this symmetry. Magnetic field applied along the $[001]$ direction ($1'$ axis) leads to compression strain $\lambda_{1'}(H)$ along this axis and tensile strain along $2'$ axis ($[010]$ direction). This leads to the fact that upon application of E -field compression strains in piezoelectric results in bending along $2'$ axis and compression strain along $1'$ axis. Thus, for the film on (100) plane and H along $[001]$ direction we have for the nonzero component of the strain the following expressions:

$$\begin{aligned} {}^m S_{1'} &= d_{31} E_3 \left(\nu \frac{{}^p Y W t^p (z_0 + t^p / 2) ({}^s t + {}^m t - z_0)}{D} + \frac{{}^p Y^p t}{\bar{Y} t} \right) \\ {}^m S_{2'} &= -d_{31} E_3 \left(\frac{{}^p Y W t^p (z_0 + t^p / 2) ({}^s t + {}^m t - z_0)}{D} + \nu \frac{{}^p Y^p t}{\bar{Y} t} \right). \end{aligned} \quad (23)$$

Using the relations ${}^m S_3 = {}^m S_{1'}$ and for along $[001]$ direction $\alpha_1 = \alpha_2 = 0, \alpha_3 = 1$ and we get

for magnetoelectric constant the following expression:

$$A_{[001]}^{(100)} = \frac{3^m Y d_{31}}{M_s (1+\nu)} \lambda_{100} \left[\nu \frac{{}^p Y W t^p (z_0 + t^p / 2) ({}^s t + {}^m t - z_0)}{D} + \frac{{}^p Y^p t}{\bar{Y} t} \right] \quad (24)$$

For the angle $\phi = 31^\circ$, using Eq. (9) we obtained

$$A_{31}^{(100)} = \frac{3^m Y d_{31}}{M_s (1+\nu)} \lambda_{100} \left[((1+\nu) \cos^2 \phi - 1) \frac{{}^p Y W t^p (z_0 + t^p / 2) ({}^s t + {}^m t - z_0)}{D} + ((1-\nu) \cos^2 \phi + \nu) \frac{{}^p Y {}^p t}{\bar{Y} t} \right] \quad (25)$$

Next, for comparison with experiment, we estimated the A -values for NFO/MGO/PZT with the following values for the material parameters [29,32-34]:

$$\begin{aligned} & {}^p c_{11} = 12.6 \times 10^{10} \text{ N/m}^2, \quad {}^p c_{12} = 7.95 \times 10^{10} \text{ N/m}^2, \\ \text{PZT: } & {}^p c_{13} = 8.4 \times 10^{10} \text{ N/m}^2, \quad {}^p c_{33} = 11.7 \times 10^{10} \text{ N/m}^2, \quad d_{31} = -175 \times 10^{-12} \text{ m/V}; \end{aligned}$$

$$\begin{aligned} & {}^m c_{11} = 21.99 \times 10^{10} \text{ N/m}^2, \quad {}^m c_{12} = 10.94 \times 10^{10} \text{ N/m}^2, \\ \text{NFO: } & {}^m c_{44} = 8.12 \times 10^{10} \text{ N/m}^2, \quad \lambda_{111} = -15 \times 10^{-6}, \quad \lambda_{100} = -40 \times 10^{-6}; \end{aligned}$$

$$\begin{aligned} \text{MGO: } & {}^s c_{11} = 28.6 \times 10^{10} \text{ N/m}^2, \quad {}^s c_{12} = 8.7 \times 10^{10} \text{ N/m}^2, \\ & {}^s c_{44} = 14.8 \times 10^{10} \text{ N/m}^2 \end{aligned}$$

$${}^s t = 0.5 \text{ mm}, \quad {}^p t = 0.2 \text{ mm}, \quad {}^m t = 600 \text{ nm},$$

The estimated A - values for PZT/NFO/(110) MGO are given in Section 4.

References

1. W. Eerenstein, N. D. Mathur, and James F. Scott. "Multiferroic and magnetoelectric materials." *Nature* 442, 759 (2006).
2. Ce-Wen Nan, M. I. Bichurin, Shuxiang Dong, D. Viehland, and G. Srinivasan. "Multiferroic magnetoelectric composites: Historical perspective, status, and future directions." *Journal of Applied Physics* 103, 031101 (2008).
3. C. Vaz, Jason Hoffman, Charles H. Ahn, and Ramamoorthy Ramesh. "Magnetoelectric coupling effects in multiferroic complex oxide composite structures." *Advanced Materials* 22, 2900 (2010).
4. J. Ma, Jiamian Hu, Zheng Li, and Ce-Wen Nan. "Recent progress in multiferroic magnetoelectric composites: from bulk to thin films." *Advanced Materials* 23, 1062 (2011).
5. N. A. Spaldin, "Multiferroics: Past, present, and future." *MRS bulletin* 42, 385 (2017).
6. H. Palneedi, Venkateswarlu Annapureddy, Shashank Priya, and Jungho Ryu. "Status and perspectives of multiferroic magnetoelectric composite materials and applications." *Actuators*, 5, 9 (2016).
7. G. Srinivasan, Gopalan, Shashank Priya, and N. Sun. *Composite magnetoelectrics: materials, structures, and applications*. Woodhead Publishing Series in Electronic and Optical Materials, No. 62, Elsevier, 2015.
8. D. Viehland, Jie Fang Li, Yaodong Yang, Tommaso Costanzo, Amin Yourdkhani, Gabriel Caruntu, Peng Zhou et al. "Tutorial: Product properties in multiferroic nanocomposites." *Journal of Applied Physics* 124, 061101 (2018).

9. L. Y. Fetisov, I. A. Baraban, Yuri K. Fetisov, D. A. Burdin, and M. M. Vopson. "Nonlinear magnetoelectric effects in flexible composite ferromagnetic–piezopolymer structures." *Journal of Magnetism and Magnetic Materials* 441 628 (2017).
10. M. Vopson, Melvin M. "Fundamentals of multiferroic materials and their possible applications." *Critical Reviews in Solid State and Materials Sciences* 40, 223 (2015).
11. C. M. Leung, Jiefang Li, D. Viehland, and X. Zhuang. "A review on applications of magnetoelectric composites: from heterostructural uncooled magnetic sensors, energy harvesters to highly efficient power converters." *Journal of Physics D: Applied Physics* 51, 263002 (2018).
12. Z. Hu, Tianxiang Nan, Xinjun Wang, Margo Staruch, Yuan Gao, Peter Finkel, and Nian X. Sun. "Voltage control of magnetism in FeGaB/PIN-PMN-PT multiferroic heterostructures for high-power and high-temperature applications." *Applied Physics Letters* 106, 022901 (2015).
13. J. F. Scott, Donald M. Evans, J. Marty Gregg, and Alexei Gruverman. "Hydrodynamics of domain walls in ferroelectrics and multiferroics: Impact on memory devices." *Applied Physics Letters* 109, 042901 (2016).
14. H. Lin, Michael R. Page, Michael McConney, John Jones, Brandon Howe, and Nian X. Sun. "Integrated magnetoelectric devices: Filters, pico-Tesla magnetometers, and ultracompact acoustic antennas." *MRS Bulletin* 43, 841 (2018).
15. S. Liu, Lianwen Deng, Shuoqing Yan, Heng Luo, Lingling Yao, Longhui He, Yuhan Li, Mingzhong Wu, and Shengxiang Huang. "Magnetoelectric properties of lead-free (80Bi0.

- 5Na_{0.5}TiO₃-20Bi_{0.5}K_{0.5}TiO₃-Ni_{0.8}Zn_{0.2}Fe₂O₄ particulate composites prepared by in situ sol-gel." *Journal of Applied Physics* 122, 034103 (2017).
16. Y. Wang, Jiefang Li, and D. Viehland. "Magnetolectrics for magnetic sensor applications: status, challenges and perspectives." *Materials Today* 17, 269 (2014).
17. L. Y. Fetisov, Vladimir N. Serov, Dmitri V. Chashin, Sergey A. Makovkin, G. Srinivasan, D. Viehland, and Yuri K. Fetisov. "A magnetoelectric sensor of threshold DC magnetic fields." *Journal of Applied Physics* 121, 154503 (2017).
18. M. Li, Alexei Matyushov, Cunzheng Dong, Huaihao Chen, Hwaider Lin, Tianxiang Nan, Zhenyun Qian, Matteo Rinaldi, Yuanhua Lin, and Nian X. Sun. "Ultra-sensitive NEMS magnetoelectric sensor for picotesla DC magnetic field detection." *Applied Physics Letters* 110, 143510 (2017).
19. X. Zhuang, C. M. Leung, J. Li, and D. Viehland. "Power conversion process in magnetoelectric gyrators." *Applied Physics Letters* 111, 103902 (2017).
20. H. Lin, Jing Lou, Yuan Gao, Ryusuke Hasegawa, Ming Liu, Brandon Howe, John Jones, Gail Brown, and Nian X. Sun. "Voltage tunable magnetoelectric inductors with improved operational frequency and quality factor for power electronics." *IEEE Transactions on Magnetics* 51, 4002705 (2015).
21. A. V. Sadovnikov, A. A. Grachev, E. N. Beginin, S. E. Sheshukova, Yu P. Sharaevskii, and S. A. Nikitov. "Voltage-controlled spin-wave coupling in adjacent ferromagnetic-ferroelectric heterostructures." *Physical Review Applied* 7, 014013 (2017).

22. X. Xue, Z. Zhou, W. Hou, M. Guan, Z. Hu, and M. Liu. "Voltage Control of Magnetism Through Two-Magnon Scattering Effect for Magnetoelectric Microwave Devices." *IEEE Transactions on Magnetics* 54, 2801504 (2018).
23. N. X. Sun and Gopalan Srinivasan. "Voltage control of magnetism in multiferroic heterostructures and devices." *SPIN*, 2, 1240004 (2012).
24. J. H. Leach, H. Liu, V. Avrutin, E. Rowe, Ü. Özgür, H. Mork oc, Y-Y. Song, and M. Wu. "Electrically and magnetically tunable phase shifters based on a barium strontium titanate-yttrium iron garnet layered structure." *Journal of Applied Physics* 108, 064106 (2010).
25. S. Shastry, G. Srinivasan, M. I. Bichurin, V. M. Petrov, and A. S. Tatarenko. "Microwave magnetoelectric effects in single crystal bilayers of yttrium iron garnet and lead magnesium niobate-lead titanate." *Physical Review B* 70, 064416 (2004).
26. S. Emori, Benjamin A. Gray, Hyung-Min Jeon, Joseph Peoples, Maxwell Schmitt, Krishnamurthy Mahalingam, Madelyn Hill et al. "Coexistence of low damping and strong magnetoelastic coupling in epitaxial spinel ferrite thin films." *Advanced Materials* 29, 1701130 (2017).
27. R. C. Budhani, Satoru Emori, Zbigniew Galazka, Benjamin A. Gray, Maxwell Schmitt, Jacob J. Wisser, Hyung-Min Jeon et al. "Pseudomorphic spinel ferrite films with perpendicular anisotropy and low damping." *Applied Physics Letters* 113, 082404 (2018).
28. Singh, Amit V., Behrouz Khodadadi, Jamileh Beik Mohammadi, Sahar Keshavarz, Tim Mewes, Devendra Singh Negi, Ranjan Datta, Zbigniew Galazka, Reinhard Uecker, and Arunava Gupta. "Bulk Single Crystal-Like Structural and Magnetic Characteristics of

Epitaxial Spinel Ferrite Thin Films with Elimination of Antiphase Boundaries." *Advanced Materials* 29, no. 30 (2017): 1701222.

29. Landolt-Bornstein; Numerical data and functional relationships in science and technology, Group III, Crystal and Solid State Physics, vol 4(b), Magnetic and Other Properties of Oxides, eds. K.-H. Hellwege and A. M. Springer, Springer-Verlag, New York (1970).
30. M. I. Bichurin, I. A. Kornev, V. M. Petrov, A. S. Tatarenko, Yu. V. Kiliba, and G. Srinivasan, Theory of magnetoelectric effects at microwave frequencies in a piezoelectric-magnetostrictive multilayer composite, *Phys. Rev. B*, 64, 094409 (2001).
31. M. I. Bichurin, V. M. Petrov, Yu. V. Kiliba, and G. Srinivasan, Magnetic and magnetoelectric susceptibilities of a ferroelectric/ferromagnetic composite at microwave frequencies *Phys. Rev. B*. 66, 134404 (2002).
32. L. E. Cross, "Ferroelectric ceramics: Tailoring properties for specific applications," *Ferroelectric ceramics*. Ed. N. Setter; Birkhäuser, Basel, 1993.
33. *Physics of Ferroelectrics: A modern perspective*, Eds. K. M. Rabe, C. H. Ahn, and J. Triscone, Springer, 2007.
34. Z. Galazka, Detlef Klimm, Klaus Irmischer, Reinhard Uecker, Mike Pietsch, Rainer Bertram, Martin Naumann et al. "MgGa₂O₄ as a new wide bandgap transparent semiconducting oxide: growth and properties of bulk single crystals." *Physica Status Solidi (a)* 212, 1455 (2015).
35. R. M. Bozorth and J. G. Walker. "Magnetostriction of single crystals of cobalt and nickel ferrites." *Physical Review* 88, 1209 (1952).
36. Y. K. Fetisov and G. Srinivasan. "Electric field tuning characteristics of a ferrite-piezoelectric microwave resonator." *Applied physics letters* 88, 143503 (2006).

37. Murthy, D. V. B., and Gopalan Srinivasan. "Broadband ferromagnetic resonance studies on influence of interface bonding on magnetoelectric effects in ferrite-ferroelectric composites." *Frontiers of Physics* 7, no. 4 (2012): 418-423.
38. C. Pettiford, J. Lou, L. Russell, N. X. Sun, "Strong Magnetoelectric Coupling at Microwave Frequencies in Metallic Magnetic Film / Lead Zirconate Titanate Multiferroic Composites", *Appl. Phys. Lett.*, 92, 122506 (2008).
39. J. Lou, David Reed, C. Pettiford, M. Liu, Pengdi Han, Shuxiang Dong, N. X. Sun, "Giant microwave tunability in FeGaB/PMN-PT multiferroic composites", *Appl. Phys. Lett.* 92, 262502 (2008).
40. A. S. Tatarenko, V. Gheevarghese, and G. Srinivasan, Magnetoelectric microwave bandpass filter. *Electronics Letters*, 42, 540 (2006).
41. Ming Liu, Ogheneyunume Obi, Jing Lou, Yajie Chen, Zhuhua Cai, Stephen Stoute, Mary Espanol, Magnum Lew, Xiaodan Situ, Kate S. Ziemer, Vince G. Harris, Nian X. Sun. Giant electric field tuning of magnetic properties in multiferroic ferrite/ferroelectric heterostructures. *Advanced Functional Materials*, 19, 1826 (2009).
42. G. Srinivasan, I. V. Zavislyak, and A. S. Tatarenko, "Millimeter-wave magnetoelectric effects in bilayers of barium hexaferrite and lead zirconate titanate." *Appl. Phys. Lett.* **89**, 152508 (2006).
43. A. B. Ustinov and G. Srinivasan, "Subterahertz excitations and magnetoelectric effects in hexaferrite-piezoelectric bilayers." *Appl. Phys. Lett.* **93**, 142503 (2008).
44. A. S. Tatarenko and G. Srinivasan, "A strain engineered voltage tunable millimeter-wave ferrite phase shifter." *Mic. Optical Tech. Lett.* 53, 261 (2011).

45. M. Li, Ming Liu, Ziyao Zhou, Nian X. Sun, D. V. B. Murthy, Gopalan Srinivasan, Tonya M. Klein, Vladimir M. Petrov, and Arunava Gupta. "Electrostatic tuning of ferromagnetic resonance and magnetoelectric interactions in ferrite-piezoelectric heterostructures grown by chemical vapor deposition." *Applied Physics Letters* 99, 192502 (2011).
46. See Supplemental Material at [URL :]. This section contains (a) profiles of the scattering parameter S_{21} vs f showing ferromagnetic resonance (FMR) in the nickel ferrite films (on magnesium or cobalt gallate substrates) in composites with PZT and E - tuning of the FMR, (b) data on shift in the FMR frequency f_r with E , and (c) estimated induced anisotropy field H_{ME} due to ME interactions and its variation with E . The ME constant A determined from data on H_{ME} vs E are also provided in Tables 1 and 2 for a series of bias magnetic fields.

Supplemental Information

Magneto-Electric Interactions in Composites of Ferrite Films on Lattice-Matched Substrates and Ferroelectrics

Peng Zhou,^{1,2} Amit V. Singh,³ Z. Li,³ M. A. Popov,^{1,4} Ying Liu,^{1,2} D. A. Filippov,⁵ Tianjin Zhang,² Wei Zhang,¹ P. J. Shah,⁶ B. M. Howe,⁶ M. E. McConney,⁶ G. Srinivasan,^{1,6 a)} M. R. Page,^{6,b)} and A. Gupta^{3,c)}

¹ *Physics Department, Oakland University, Rochester, MI 48309, USA*

² *Department of Materials Science and Engineering, Hubei University, Wuhan 430062, China*

³ *Center for Materials for Information Technology, The University of Alabama, Tuscaloosa, AL 3548, USA*

⁴ *Faculty of Radiophysics, Electronics and Computer Systems, Taras Shevchenko National University of Kyiv, Kyiv, 01601, Ukraine*

⁵ *Novgorod State University, Veliky Novgorod, 173003 Russia*

⁶ *Materials and Manufacturing Directorate, Air Force Research Laboratory, Wright-Patterson Air Force Base, Dayton, OH 45433, USA*

Authors to whom correspondence should be addressed:

^a srinivas@oakland.edu; ^b michael.page.16@us.af.mil; ^c agupta@mint.ua.edu,

This section contains (a) profiles of the scattering parameter S_{21} vs f showing ferromagnetic resonance (FMR) in the nickel ferrite films (on magnesium or cobalt gallate substrates) in composites with PZT and E - tuning of the FMR, (b) data on shift in the FMR frequency f_r with E , and (c) estimated induced anisotropy field H_{ME} due to ME interactions and its variation with E .

The ME constant A determined from data on H_{ME} vs E are also provided in Tables 1 and 2 for a series of bias magnetic fields.

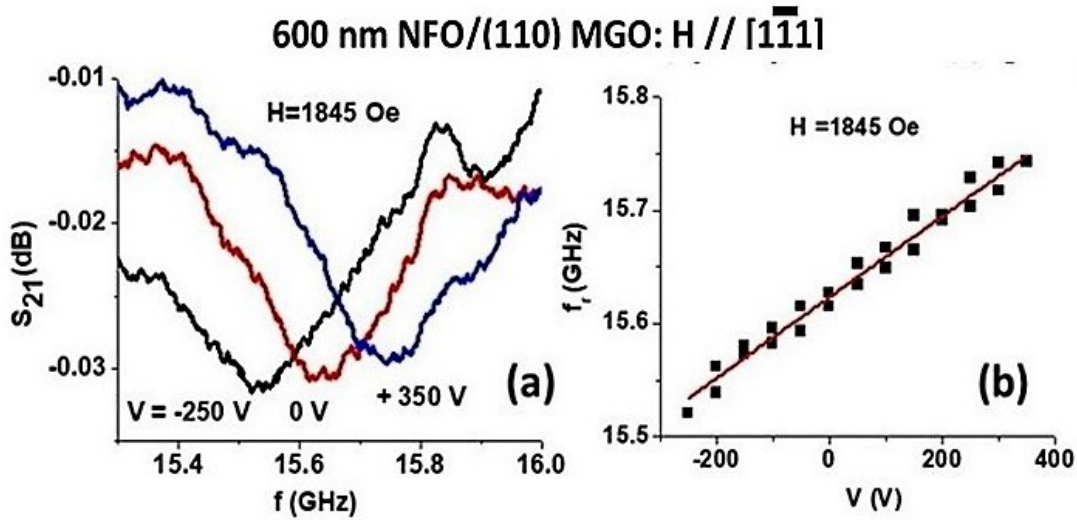


Fig.1. Results on (a) profiles of scattering matrix parameter S_{21} vs f showing FMR and (b) resonance frequency f_r vs applied voltage V across the thickness of PZT for H along $[1,-1,1]$ for composites of PZT and NFO film on (110) MGO substrate.

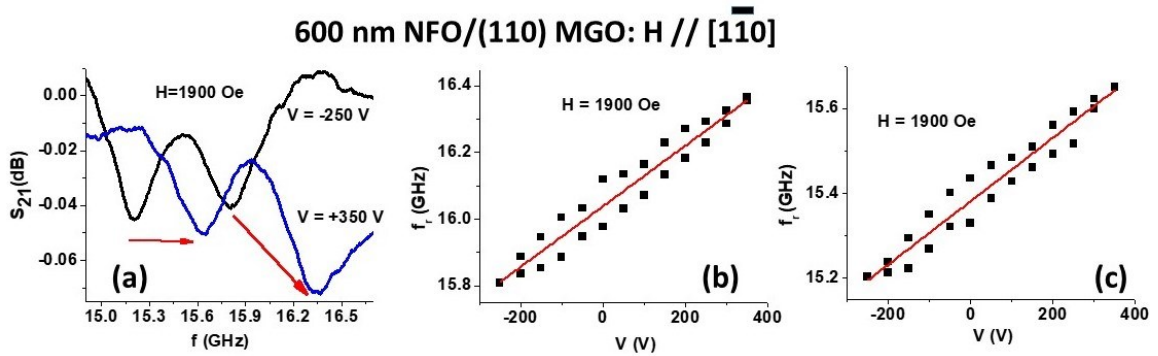


Fig.2. (a) S_{21} vs f for H along $[1,-1,0]$ for NFO on (110) MGO. The data shows two magnetic resonance modes for this case. (b) and (c) show f_r as a function of V for the two modes. But H_{ME} vs E data for the two modes and the A -values were approximately the same.

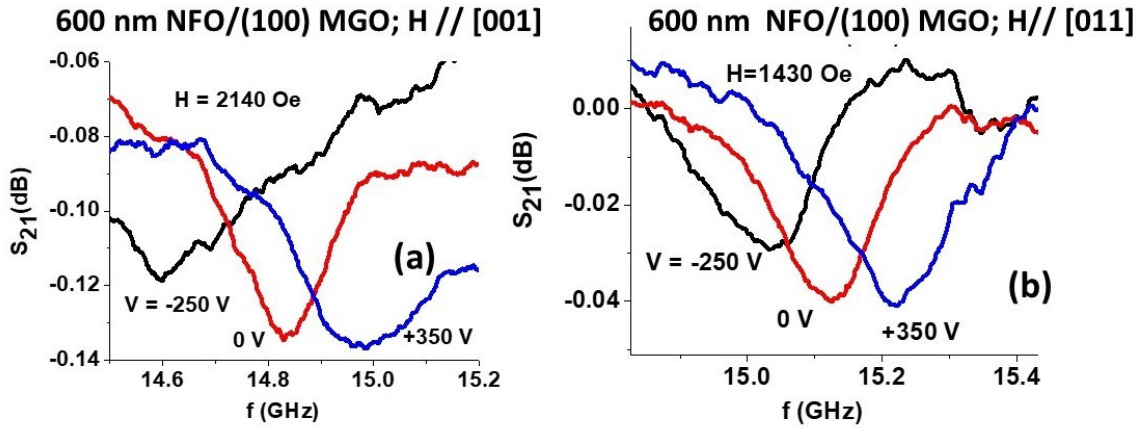


Fig.3. (a) FMR profiles for a series of applied voltage for composites with NFO on (100) MGO. The static field H was applied along the [001] direction. (b) Results on S_{21} vs f for H along [011] axis for composites with NFO film on (100) MGO substrate.

450 nm NFO/ (100) MGO

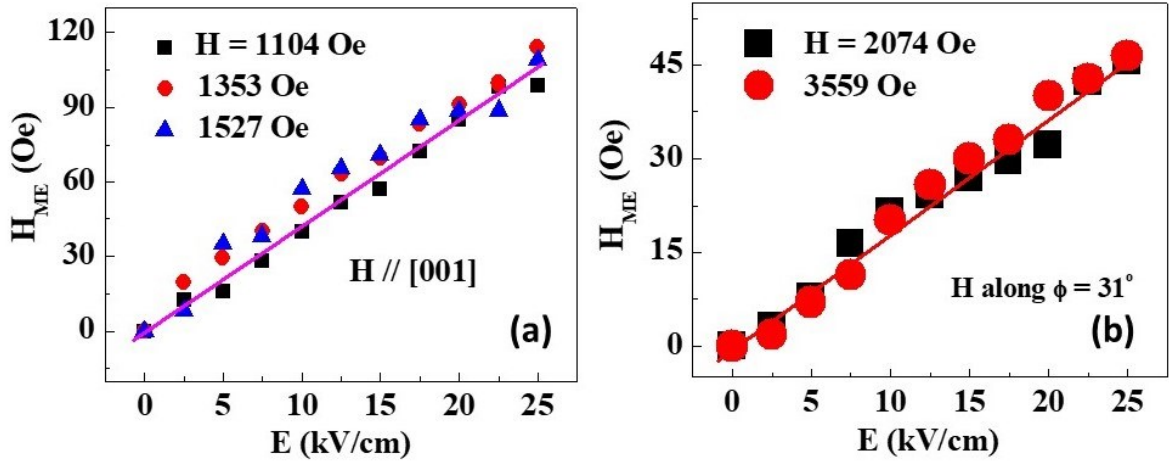


Fig.4: The E -induced ME anisotropy field H_{ME} vs E for composite with 450 nm thick NFO on (100) MGO for (a) H // [001] and (b) H in a direction 31 deg. from [001].

Table 1: Estimated ME constant A for a series of bias magnetic field H for composites with NFO films on (110) and (100) MGO.

Ferrite thickness	substrate	H orientation	H (Oe)	A (Oe cm/kV)
600 nm	(110) MGO	[001]	3240	-4.2
			3460	-3.8
		[1,-1,1]	925	2.8
			1845	2.7
		[1,-1,0]	1420	4.7
			1900	6.4
600 nm	(100) MGO	[001]	2140	4.3
			2565	4.1
			2980	5.5
		[011]	1430	2.2
			1845	2.7
450 nm	(100) MGO	[001]	1104	4.2
			1353	4.3
			1527	4.1
		$\Phi = 31^\circ$	2074	1.8
			3559	2.0

Resonance condition for $\phi = 31^\circ$

$$f = \gamma \sqrt{(H_0 + 4\pi M_{eff} + 0.61H_4 + H_{ME})(H_0 - 0.56H_4 + H_{ME})}$$

1 μm NFO/(110) CGO; H // [001]

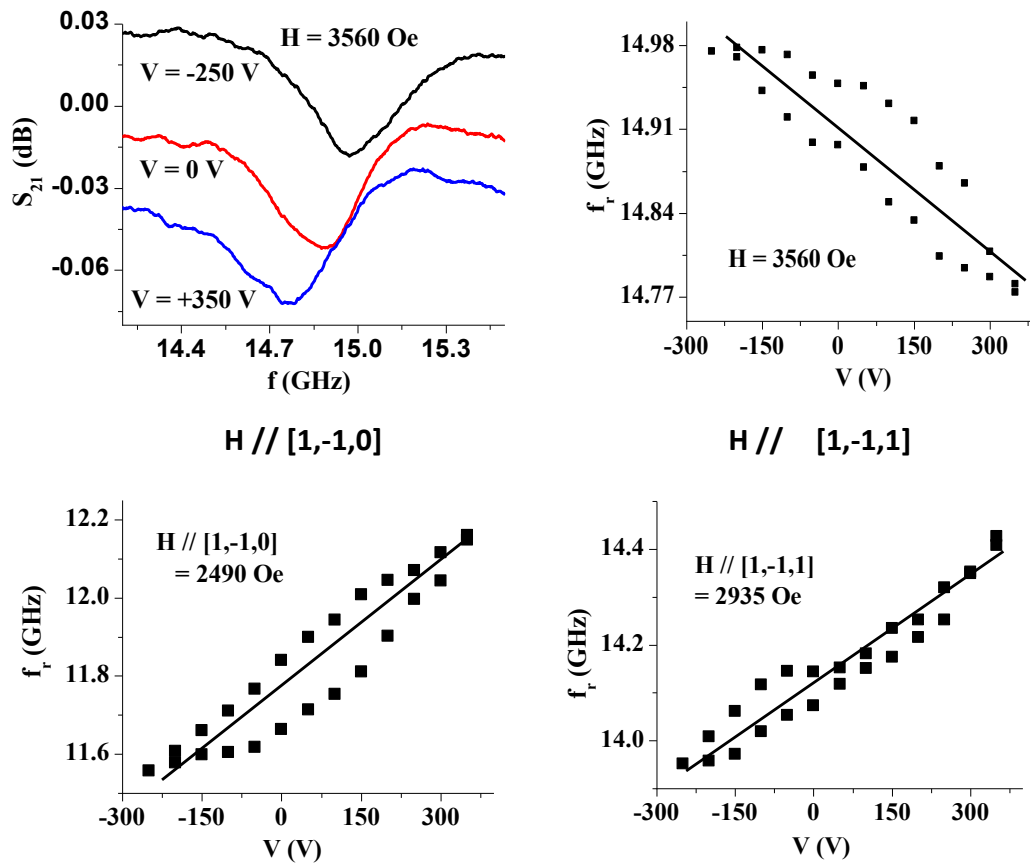


Fig.5: (Top left) Profiles of S_{21} vs f showing FMR for $H // [001]$ in composites of PZT and NFO on (110) CGO. (Top right) FMR resonance frequency f_r vs voltage V applied to PZT for $H // [001]$. The bottom figures show similar data for $H // [1,-1,0]$ and $H // [1,-1,1]$.

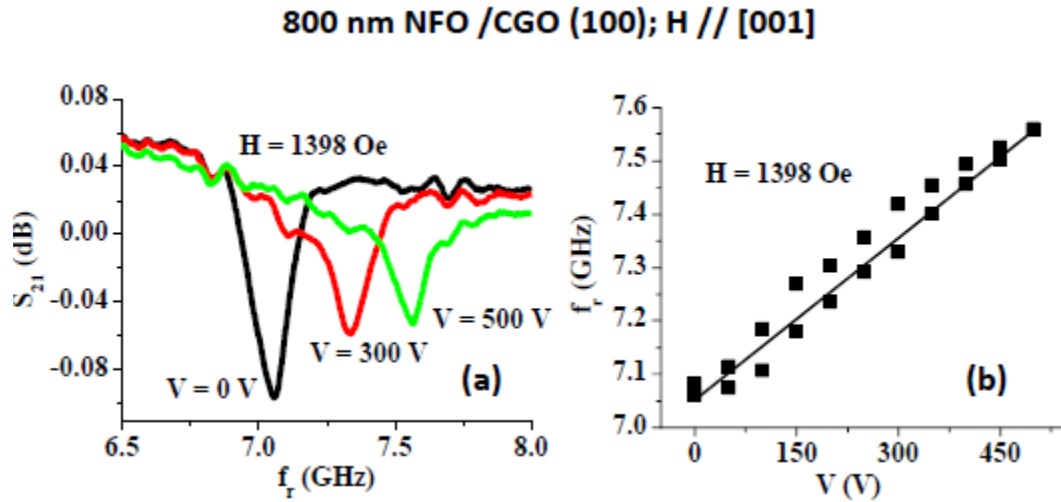


Fig.6. (a) FMR profiles for a series of applied voltage for composites with NFO on (100) CGO. The static field H was applied along the [001] direction. (b) FMR frequency f_r vs V obtained from data as in Fig.6(a).

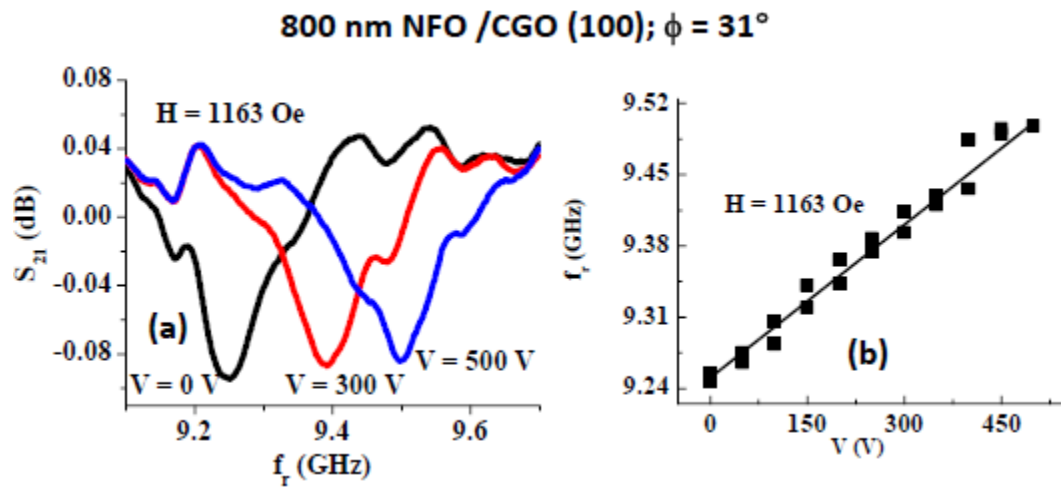


Fig.7: (a) FMR profiles for a series of applied voltage for composites with NFO on (100) CGO. The static field H was applied along 31 deg. to the [001] direction. (b) FMR frequency f_r vs V obtained from data as in Fig.7(a).

Table 2: Estimated ME constant A for a series of bias magnetic field H for composites with NFO films on (110) and (100) CGO.

Ferrite thickness	substrate	H orientation	H (Oe)	A (Oe cm/kV)
1 μm	(110) CGO	[001]	1770	-4.5
			2800	-3.7
			3560	-3.2
		[1,-1,1]	2435	7.8
			2935	6.2
			3425	6.5
		[1,-1,0]	2490	9.0
			3240	8.6
			3840	6.6
800 nm	(100) CGO	[001]	1398	5.2
		$\Phi = 31^\circ$	1163	3